Performance Analysis of PAM4 Signal Transmission in Inter-datacenter Multicore Fiber Links Impaired by Inter-Core Crosstalk

Rafael A. Dias[2], João L. Rebola[1,2] and Adolfo V. T. Cartaxo[1,2]
[1]*Optical Communications and Photonics Group, Instituto de Telecomunicações, Lisboa, Portugal*
[2]*Instituto Universitário de Lisboa (ISCTE-IUL), Lisboa, Portugal*

Keywords: Bit Error Rate, Inter-Core Crosstalk, Inter-datacenter Connections, Multicore Fiber, Outage Probability, PAM4.

Abstract: In this work, we propose to use four-level pulse amplitude modulation (PAM4) and multicore fibers (MCFs) to support very high capacity inter-datacenter connections. The limitations imposed by inter-core crosstalk (ICXT) on the performance of 112 Gb/s up to 80 km-long optically amplified PAM4 inter-datacenter links with intensity-modulation and direct-detection (IM-DD) and full chromatic dispersion compensation in the optical domain are analyzed through numerical simulation. We show that those PAM4 inter-datacenter links achieve an outage probability (OP) of 10^{-4} with a maximum ICXT level of -13.9 dB for high skew-symbol rate products and require an ICXT level decrease of about 8.1 dB to achieve the same OP for low skew-symbol rate products. Due to using full dispersion compensation, the OP is not much affected by increasing the MCF length, from 10 km, where electrical noise significantly contributes to the performance degradation, to 80 km, where signal-amplified spontaneous emission beat noise is dominant. For an OP of 10^{-4}, the maximum acceptable ICXT level shows only a 1.4 dB variation with the MCF length increase.

1 INTRODUCTION

Nowadays, datacenters provide a vital infrastructure to Internet online services and in the last few years, worldwide traffic in optical networks has been increasing dramatically around 30% per year (Cisco, 2018), (Klaus et al., 2017). This growth is fuelled by the progressive development of next-generation 5G mobile broadband technologies, expansion of the Internet of things, and increasing of high-data-rate applications such as streaming video, real-time gaming, cloud computing, and big data analysis (Klaus et al., 2017). This growth is demanding a higher capacity in datacenters. To accomplish such demands, cloud companies and content providers have built multiple datacenters in different locations which are separated by large distances because this approach offers multiple benefits (increased availability, reduced latency to customers) for distributed applications with a wide range of users such as email, multimedia services, social networks and online storage (Noormohammadpour and Raghavendra, 2018). Moreover, the traffic which was mainly transmitted only from external datacenters to servers was surpassed by the amount of traffic exchanged between servers inside the same and between datacenters (Cisco, 2018).

In intra-datacenter optical fiber links, the format of the signals usually transmitted was the on-off keying (OOK), where intensity-modulation and direct-detection (IM-DD) ensured low cost and complexity (Zhou et al., 2019). However, in 2014, OOK signal transmission reached its limit at the data rate of 25 Gb/s (Perin et al., 2018). To surpass the limitation imposed by OOK modulation, PAM4 signal transmission has been introduced for datacenter communications in 2017 (Zhou et al., 2019), (Kachris and Tomkos, 2012). The PAM4 modulation format reduces the signal bandwidth by half and doubles spectral efficiency in comparison to OOK signals. Therefore, PAM4 is expected to be an economical and efficient enabler of 100G and 400G single-channel transmission in intra and inter-datacenter connections (Zhou et al., 2019), (Perin et al., 2018).

Multicore fibers (MCFs) have been recently proposed to increase the capacity of short-haul links, such as datacenters interconnects, and as they can be more densely packed, space can be saved inside datacenter facilities in comparison with the space occupied by multiple bundles of single-core single-mode fibers (SC-SMF) required to achieve the same capacity (Butler et al., 2017). Weakly-coupled MCFs provide an economic solution for the required capacity, as individual cores can be used as independent channels with similar propagation delays. However, the effect of inter-core crosstalk (ICXT) limits the MCF reach and performance (Rebola et al., 2019b), (Jorge et al., 2020).

Dias, R., Rebola, J. and Cartaxo, A.
Performance Analysis of PAM4 Signal Transmission in Inter-datacenter Multicore Fiber Links Impaired by Inter-Core Crosstalk.
DOI: 10.5220/0010321000940103
In *Proceedings of the 9th International Conference on Photonics, Optics and Laser Technology (PHOTOPTICS 2021)*, pages 94-103
ISBN: 978-989-758-492-3

The ICXT effect is reasonably well studied in the literature (Luís et al., 2016), (Cartaxo et al., 2016), (Alves and Cartaxo, 2019) and, due to the random evolution of ICXT over time, ICXT-impaired systems may experience: (i) random variations of the bit error rate (BER) over short time periods (Alves et al., 2019), (Alves and Cartaxo, 2017), and (ii) system outage over long time periods due to high ICXT levels (Alves et al., 2019). Therefore, it is essential to study the outage probability (OP) and bit error rate (BER) in PAM4 IM-DD systems supported by MCFs and limited by ICXT (Rebola et al., 2019b).

In this work, the performance of IM-DD inter-datacenter links with full loss and perfect dispersion compensation and PAM4 signal transmission up to 80 km is analyzed taking the limitations imposed by ICXT into account.

2 SYSTEM MODEL

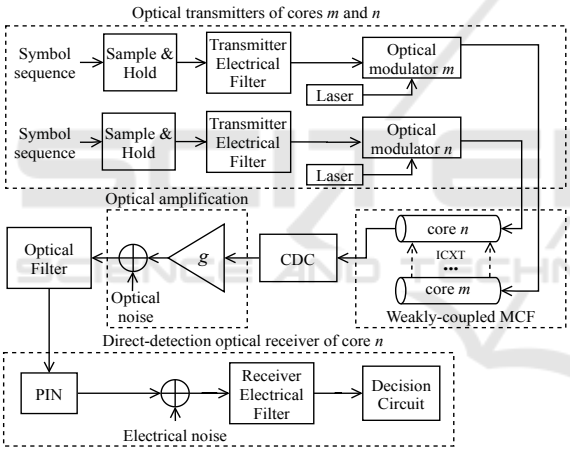

Figure 1: Equivalent model of an optically amplified inter-datacenter link supported by MCFs and with CD compensation.

Inter-datacenter links can reach up to 100 km and usually operate at 1550 nm to enable amplification using erbium-doped fiber amplifiers (EDFAs). In these links, due to the higher distances in comparison with shorter intra-datacenter links, chromatic dispersion (CD) becomes significant and must be reduced by using dispersion compensation techniques (Perin et al., 2018), (El-Fiky et al., 2017). Typically, inter-core datacenter links are supported by single-mode single-core fibers (SM-SCFs). In this work, our proposal to increase significantly the link capacity is to use weakly-coupled MCFs to support such links.

The system equivalent model used in this work to study the ICXT impact on the performance of inter-datacenter links supported by MCFs is shown in Fig. 1. It is composed of two transmitters (TXs), one for the interfering core and the other for the interfered core, each one generating a different PAM4 signal. After symbols generation, the PAM4 symbols are sampled and passed through an electrical filter that models the frequency limitations of the electrical part of the transmitter. Each optical modulator is assumed without chirp and with a finite extinction ratio.

The weakly-coupled MCF model considers an interfered core n and a single interfering core m, and linear signal propagation. The ICXT is described by the dual-polarization discrete changes model (DP-DCM) with two cores (Soeiro et al., 2017). The attenuation coefficient and dispersion parameters of the two cores are assumed equal. At the output of the interfered core n, the ICXT induced by core m is added to the signal transmitted in core n. As the objective of this work is to analyze the impact of ICXT on the performance of very high capacity inter-datacenter links, the chromatic dispersion compensation (CDC) module uses a dispersion compensating fiber (DCF), designed to fully compensate the dispersion induced by core n. An inter-datacenter link fully supported by multicore technology would be the most feasible and practical solution, however to the authors' best knowledge, MC-DCFs are not an available technology. Our proposed solution is to use a spatial demultiplexer at the MCF output followed by a CDC module composed by a bundle of parallel single-core DCFs, each one designed to compensate the CD induced in a specific fiber core of the MCF. After the CDC, the PAM4 signal impaired by ICXT is optically amplified by an EDFA and an optical filter is used to suppress amplified spontaneous emission (ASE) noise generated by the EDFA. The EDFA gain is designed to fully compensate the losses introduced by the MCF and DCF. The direct-detection optical receiver includes a PIN photodetector, electrical noise addition due to circuitry of the electrical part of the receiver, electrical filtering, and the decision circuit to decide on the transmitted PAM4 symbol. In the following, a detailed description of these models is presented.

2.1 PAM4 Signal Characterization

In this subsection, the generation and characterization of the PAM4 signal generated at the output of the optical transmitters is explained. In the simulator, the PAM4 symbols sequence is generated using deBruijn sequences of maximum length $4^{N_{reg}}$, obtained from Galois arithmetic, where N_{reg} represents the length of the offset register used to generate the sequence. The symbols '0', '1', '2' and '3' are equally likely to occur (Rebola and Cartaxo, 2000). Fig. 2 shows a rep-

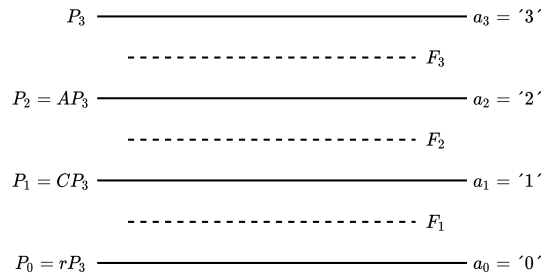

Figure 2: Representation of the ideal power levels of an optical PAM4 signal with non-zero extinction ratio and the corresponding decision thresholds.

resentation of the ideal PAM4 signal power levels for a non-zero extinction ratio where a_k, with k=0, 1, 2 and 3 correspond to the PAM4 signal symbols; F_1, F_2 and F_3, are the ideal decision thresholds; P_0, P_1, P_2 and P_3 are the powers corresponding to each of the symbols a_k, and r is the extinction ratio defined as $r = P_0/P_3$. The constants A and C define the intermediate levels of the PAM4 signal (Rebola and Cartaxo, 2000). In optically amplified links, signal-amplified spontaneous emission (ASE) beat noise typically dominates the performance degradation and leads to different received noise powers proportional to the different intensity levels of the signal (Perin et al., 2018). In (Rebola and Cartaxo, 2000), the optimization of A and C is studied to minimize the bit error probability for optically amplified PAM4 links where signal-ASE is dominant. The optimal A and C are given by $C = (1+4\sqrt{r}+4r)/9$ and $A = (4+4r+r)/9$ (Rebola and Cartaxo, 2000). After generation, the ideal PAM4 signal is filtered by a 3^{rd} order Bessel filter to model the amplitude and phase distortion induced by the filtering and parasitics at the electrical part of the transmitter. The -3 dB bandwidth of the Bessel filter is set equal to the symbol rate R_s.

2.2 Discrete Changes Model

In this subsection, the simulation model known as DP-DCM, used to characterize the ICXT induced by the cores of the MCF is described with more detail (Soeiro et al., 2017). The DP-DCM characterizes the ICXT induced by the different cores of the MCF on the interfered core. The ICXT was reported to result mostly from the discrete contribution of phase matching points (PMPs). The PMPs are points along the longitudinal propagation direction of the fiber for which the difference between the effective refractive index of the interfering and interfered cores is zero (Soeiro et al., 2017). These points manifest randomly along the fiber and the total ICXT can be approximated as the sum of the contributions associated with each PMP. Each contribution is weighted by an independent random phase shift (RPS) and the corresponding propagation delay (Rademacher et al., 2017). The RPSs model random variations of the bending radius, twist rate, or other conditions in the MCF (Soeiro et al., 2017), (Cartaxo et al., 2016). It should be highlighted that this model provides a very good characterization of the ICXT impact in IM-DD optical communication systems, as shown in (Soeiro et al., 2017), by comparison with experimental results (Alves et al., 2019) (Alves and Cartaxo, 2017) (Alves and Cartaxo, 2019).

The DP-DCM describes the ICXT in the two polarization directions **x** and **y**. The transfer functions $F_{a,b}(\omega)$, model the frequency response of the ICXT from the polarization a (with $a = x$ or y) at the input of core m to the polarization b (with $b = x$ or y) at the output of core n and are given by (Soeiro et al., 2017)

$$F_{a,b}(\omega) = -\frac{j}{\sqrt{2}}\overline{K}_{nm}\exp\left(-j\overline{\beta}_n(\omega)L\right)\exp\left(-\frac{\alpha_n}{2}L\right) \sum_{k=1}^{N_p}\exp\left[-j(\overline{\beta}_m(\omega)-\overline{\beta}_n(\omega))z_k\right]\exp\left[-j\phi_{nm,k}^{(a,b)}\right] \quad (1)$$

where α_n is the power attenuation coefficient of core n, $\overline{K}_{nm}$ is the average inter-core coupling coefficient, which is given by the average of its contributions in the two polarization directions (Soeiro et al., 2017), ω is the angular frequency, L is the MCF length; N_p is the number of PMPs (Cartaxo et al., 2016), $\phi_{nm,k}^{(a,b)}$ represents the RPS associated with the k-th PMP, which is modelled by an uniform distribution between 0 and 2π, $\overline{\beta}_l(\omega)$ (with $l = n$ or m) is the average of the propagation constants in the two polarization directions in cores l, which is given by (Agrawal, 2010)

$$\overline{\beta}_l(\omega) = \beta_{0,l} + \beta_{1,l}\omega + \frac{\beta_{2,l}}{2}\omega^2 + \frac{\beta_{3,l}}{6}\omega^3 \quad (2)$$

where $\beta_{0,l}$ is the propagation constant at the operating wavelength λ_0, $\beta_{1,l}$ is the inverse of the group velocity, $\beta_{2,l}$ is the group velocity dispersion and $\beta_{3,l}$ is the higher order dispersion, for core l. The skew between the interfering core, m and the interfered core, n, is given by $S_{mn} = d_{mn}L$, where d_{mn} is the walkoff between cores m and n defined by $d_{mn} = \beta_{1,m} - \beta_{1,n}$.

The longitudinal coordinate of the k-th PMP, z_k, is randomly distributed between two consecutive PMPs and is given by $z_k = [L(r_k + k - 1)]/N_p$, where r_k $(1 \leq k \leq N_p)$ are independent random variables with uniform distribution in the interval $[0, 1[$.

The DP-DCM has been developed to keep the complexity and time of simulation at acceptable levels. In such a model, the evolution of the ICXT impact on the system performance is evaluated in time fractions with a much shorter duration than the ICXT decorrelation time. Those time fractions are separated by time

intervals longer than the decorrelation time of ICXT. This means that from time fraction to time fraction, the ICXT is uncorrelated and, within each time fraction, is totally correlated. For this reason, each time fraction corresponds to an independent set of RPSs, which we name MCF realization. Therefore, the different MCF realizations are obtained by generating randomly different sets of N_p RPSs. In each iteration of the Monte Carlo (MC) simulator, one MCF realization is generated, and the symbols of the PAM4 signal transmitted in core m are randomly generated. For equal powers at the input of the interfered and interfering cores and identical loss in the two cores, the ratio between the mean ICXT power and the mean power of the signal, at the output of the interfered core n, named ICXT level, X_c, is related to the parameters of Eq. 1 by $X_c = N_p|K_{nm}|^2$ (Soeiro et al., 2017).

2.3 Chromatic Dispersion Compensation Modeling

To compensate the dispersion introduced along the transmission through core n, a DCF is used at the output of the MCF to fully compensate the distortion due to chromatic dispersion on the signal impaired by ICXT. The DCF is modelled considering linear propagation transmission, with α_{DCF} characterizing the DCF attenuation coefficient. The DCF length is designed to fully compensate the accumulated dispersion induced by the MCF at the operating wavelength, by setting the DCF length to $L_{DCF} = -D_{\lambda,n}L/D_{\lambda,DCF}$ (Agrawal, 2010), where $D_{\lambda,n}$ is the core n dispersion parameter and $D_{\lambda,DCF}$ is the DCF dispersion parameter.

2.4 Optical Amplification and Filtering Modelling

In this work, the EDFA gain output is designed to fully compensate the losses introduced by the MCF and DCF. The ASE noise is modelled as additive white Gaussian noise with power spectral density, per polarization mode, given by $S_{ASE} = 0.5F_n(g-1)h\nu_o$ (Agrawal, 2010), where g is the amplifier gain output in linear units, $h\nu_o$ is the photon energy, and F_n is the amplifier noise figure.

The optical filter is modelled by a 4^{th} order super Gaussian (SG) filter. The transfer function of the n-th order SG filter is given by

$$H_o(f) = \frac{1}{\sqrt{i_L}} \exp\left[-\left(\frac{2|f-f_o|}{B_o}\right)^{2n} \ln\sqrt{2}\right] \quad (3)$$

where f_o and i_L are the optical filter central frequency and insertion loss in linear units, and B_o is the optical filter bandwidth at -3 dB.

2.5 Optical Receiver

At the optical receiver, the PIN photodetector is modelled as a square-law device with responsivity R_λ. The electrical filter of the optical receiver is modelled as 3^{rd} order Bessel filter with a -3 dB bandwidth, $B_{e,RX}$. The electrical noise power after the receiver electrical filter is given by $\sigma_c^2 = R_\lambda^2 NEP^2 B_{e,n}$ (Agrawal, 2010), where NEP is the noise equivalent power, defined as the minimum optical power necessary to generate a photocurrent equal to the noise current of the photodetector (Agrawal, 2010). The bandwidth $B_{e,n}$ is the noise equivalent bandwidth of the receiver electrical filter.

The detected ASE noise power for the k-th received PAM4 symbol at the electrical filter output, is given by $\sigma_{n,k,ASE}^2 = 4S_{ASE}B_{e,n}R_\lambda^2(gP_k + B_{o,n}S_{ASE})$ (Rebola and Cartaxo, 2000), where P_k is the symbol level corresponding to the received a_k symbol taken from the eye-pattern and $B_{o,n}$ is the noise equivalent bandwidth of the optical filter. At the decision circuit input, the received signal impaired by ICXT, residual dispersion, ASE and electrical noises is processed to estimate the BER and OP.

2.6 BER and OP Calculation

In this subsection, the procedure for the BER and OP estimation in IM-DD PAM4 systems impaired by ICXT is described. The BER is calculated by the semi-analytical method known as the exhaustive Gaussian approach, which, for a PAM4 received signal is given by (Rebola and Cartaxo, 2000)

$$BER = \frac{1}{2\cdot 4^{N_{reg}}}\left\{\sum_{\substack{k=1\\a_k=0}}^{4^{N_{reg}}} Q\left(\frac{F_1 - i_{0,k}}{\sigma_{0,k}}\right) + \sum_{\substack{k=1\\a_k=1}}^{4^{N_{reg}}}\left[Q\left(\frac{i_{1,k}-F_1}{\sigma_{1,k}}\right) + Q\left(\frac{F_2 - i_{1,k}}{\sigma_{1,k}}\right)\right] + \sum_{\substack{k=1\\a_k=2}}^{4^{N_{reg}}}\left[Q\left(\frac{i_{2,k}-F_2}{\sigma_{2,k}}\right) + Q\left(\frac{F_3 - i_{2,k}}{\sigma_{2,k}}\right)\right] + \sum_{\substack{k=1\\a_k=3}}^{4^{N_{reg}}} Q\left(\frac{i_{3,k}-F_3}{\sigma_{3,k}}\right)\right\} \quad (4)$$

where $i_{0,k}$, $i_{1,k}$, $i_{2,k}$ and $i_{3,k}$ are the means of the currents at the input of the decision circuit for the symbols '0', '1', '2' and '3', respectively, at the time sampling

instants, $t_k = t_o + T_s(k-1)$, where T_s is the symbol period; t_o is extracted from the received eye-pattern at the decision circuit input and $k \in \{1, ..., 4^{N_{reg}}\}$, $\sigma_{0,k}$, $\sigma_{1,k}$, $\sigma_{2,k}$ and $\sigma_{3,k}$ are the noise standard deviations of the same current for the different time sampling instants (Rebola and Cartaxo, 2000). The $Q(x)$ function is given by (Carlson and Crilly, 2010)

$$Q(x) = \int_x^{\infty} \frac{1}{\sqrt{2\pi}} e^{-\frac{\xi^2}{2}} d\xi \quad (5)$$

In the simulation, the decision thresholds F_1, F_2 and F_3 are optimized by applying the bisection method to minimize the BER. The effect of intersymbol interference from filtering and fiber dispersion is taken into account by the waveform distortion in the eye pattern at these t_k sampling time instants and in Eq. 4, this effect is included in the mean currents $i_{0,k}$, $i_{1,k}$, $i_{2,k}$ and $i_{3,k}$. The effect of ICXT on the interfered core is also taken into account in these mean currents by the waveform distortion induced on the receiver signal. The effect of electrical noise, signal-ASE, and ASE-ASE beat noises are taken into account semi-analytically in the standard deviations of the received symbols, $\sigma_{0,k}$, $\sigma_{1,k}$, $\sigma_{2,k}$ and $\sigma_{3,k}$.

The OP is the probability of a system becoming unavailable, i.e., the probability of the BER in the presence of ICXT surpasses a given BER limit. In the simulation, the OP is estimated by $OP = N_o/Nr$ (Winzer and Foschini, 2011), (Rebola et al., 2019b), where N_o is the number of occurrences of BER above the BER limit and N_r is the number of simulated MCF realizations necessary to reach N_o occurrences of BER above the BER limit. The required outage probability in optical communications is typically lower than 10^{-4} (Winzer and Foschini, 2011), (Cvijetic et al., 2008).

3 NUMERICAL RESULTS AND DISCUSSION

In this section, the impact of ICXT on the performance of the transmission of PAM4 signals in optically amplified IM-DD links, emulating inter-datacenter connections is assessed. The system simulation parameters used throughout these studies are presented in Table 1.

The DCF dispersion slope was set to compensate for the effect of the MCF dispersion slope. The electrical and optical receiver filters bandwidth were optimized in a back-to-back configuration to minimize the receiver sensitivity. Then, for each link length, the signal power at the transmitter output has been set to achieve the BER of 3.8×10^{-5} in absence of ICXT, which is two orders of magnitude below the BER limit in presence of ICXT. A similar assumption was considered in (Rebola et al., 2019c). In this work, we consider a target BER limit of 3.8×10^{-3} in presence of ICXT, since it is the most commonly used for datacenters connections with forward-error correction (El-Fiky et al., 2017), (Xing et al., 2018). The number of PMPs is chosen to be high enough (1000) to characterize the ICXT statistics rigorously (Cartaxo et al., 2016). Two different inter-core skews are analysed: i) $|S_{mn} \cdot R_s| \gg 1$, the symbol rate of the PAM4 signal is much higher than the ICXT decorrelation bandwidth, which is proportional to the inverse of the skew (Alves and Cartaxo, 2019) and the ICXT creates amplitude levels in the received eye-pattern that seem to exhibit a "noise"-like behavior (Rebola et al., 2019a), and ii) $|S_{mn} \cdot R_s| \ll 1$, where the symbol rate of the PAM4 signal is much lower than the ICXT decorrelation bandwidth (Alves and Cartaxo, 2019) and well-defined amplitude levels in the eye-patterns are created due to ICXT (Rebola et al., 2019a).

Table 1: System and simulation parameters.

Parameters	Value
Operation wavelength	$\lambda_0 = 1550$nm
$B_{e,RX}$	$0.85 \times R_s$
B_o	$1.6 \times R_s$
Symbol rate	$R_s = 56$ Gbaud
Number of generated PAM4 symbols in each MCF realization	$N = 4^4$
Number of PMPs	$N_p = 1000$
Skew-symbol rate product	$\lvert S_{mn} \cdot R_s \rvert$=1000, $\lvert S_{mn} \cdot R_s \rvert$=0.01
MCF chromatic dispersion parameter	$D_{\lambda,n}$ =17 $\frac{\text{ps}}{\text{nm km}}$
MCF attenuation coefficient	α_n=0.2 dB/km
DCF chromatic dispersion parameter	$D_{\lambda,DCF}$ =-100 $\frac{\text{ps}}{\text{nm km}}$
DCF attenuation coefficient	α_{DCF}=0.5 dB/km
BER limit	3.8×10^{-3}
BER in absence of ICXT	3.8×10^{-5}

In the following subsections, the impact of the ICXT on the average BER and received eye-pattern is assessed for a MCF length of 10 km and the OP is assessed for a MCF length of 10, 40 and 80 km.

3.1 BER in Each MCF Realization

The average BER is computed in each MCF realization by averaging the BERs per realization calculated in previous MCF realizations. In Figs. 3 a) and b), the

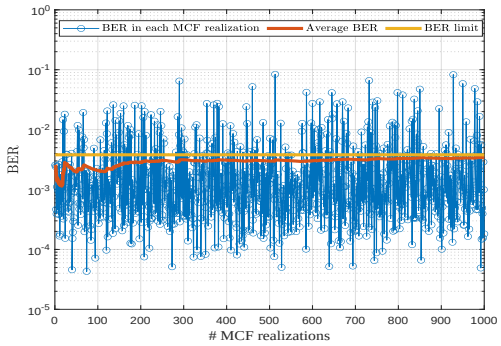

(a) $|S_{mn}{\cdot}R_s|$=1000, $X_c = -14$ dB

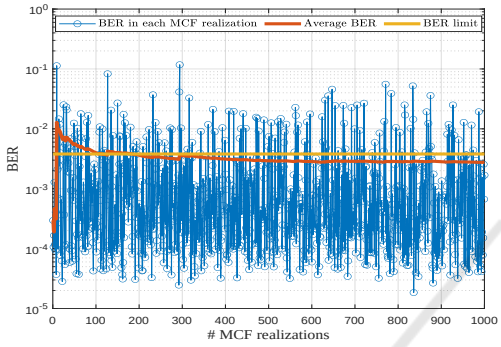

(b) $|S_{mn}{\cdot}R_s|$=0.01, $X_c = -16$ dB

Figure 3: BER in each MCF realization and average BER as a function of the number of MCF realizations, for $r = 0$.

average BER is stabilized at 3.4×10^{-3} and 2.7×10^{-3}, respectively, after 1000 MCF realizations. This number of MCF realizations is a conservative choice to achieve stabilized values of the average BER. A similar conclusion was shown in (Rebola et al., 2019c), for OOK systems. Fig. 3 shows that, with low $|S_{mn}{\cdot}R_s|$ and $X_c = -16$ dB, the BER limit is exceeded about 187 times, i.e., there are 187 occurrences of the BER that lead to system outage. The OP, in this case, is approximately 0.187. With high $|S_{mn}{\cdot}R_s|$ and $X_c = -14$ dB, the BER limit is exceeded about 145 times, which indicates an approximated OP of 0.145. After this analysis, it is possible to infer that for $|S_{mn}{\cdot}R_s|$=1000, the performance of the PAM4 inter-datacenter link is less impaired by ICXT, than for $|S_{mn}{\cdot}R_s|$=0.01, since a 2 dB higher ICXT level is required to achieve a similar OP. Similar conclusions regarding the average BER have been obtained for links with 20 km, for OOK signalling on the interfered and interfering cores (Rebola et al., 2019c) and for PAM4 signalling in the interfered core and OOK signalling in the interfering core (Jorge et al., 2020).

The results shown in Fig. 3 indicate that, for these ICXT levels, the average BER is kept below the BER limit. However, the BER in each MCF realization surpasses the BER limit several times, which leads to system outage. The OPs estimated in Fig. 3 are considerably above the typically required OP (not exceeding 10^{-4}). This demonstrates that the OP is a more important performance metric than the average BER in these optical systems. Therefore, it is essential to study the OP in PAM4 IM-DD systems supported by MCFs impaired by ICXT.

3.2 Eye-pattern Analysis

Through the eye-pattern analysis, it is also possible to draw some conclusions regarding the impact of the ICXT on the performance of an optically amplified PAM4 IM-DD system with full loss and chromatic dispersion compensation. Fig. 4 shows the received eye-patterns at the decision circuit input for $|S_{mn}{\cdot}R_s|$=1000, $r = 0$ and $X_c = -14$ dB, for a) the best BER (4.29×10^{-5}) and b) the worst BER (8.30×10^{-2}) per MCF realization shown in Fig. 3 a). Fig. 5 shows

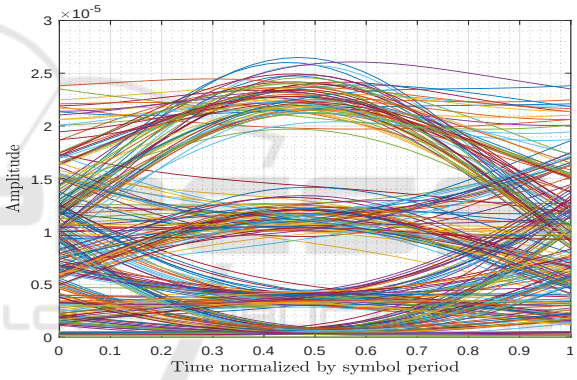

(a) BER=4.29×10^{-5}

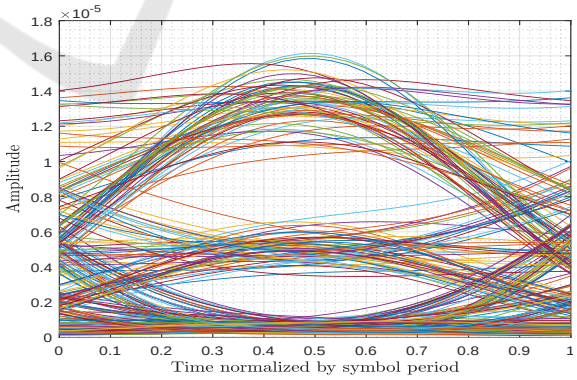

(b) BER=8.30×10^{-2}

Figure 4: Eye-Patterns at the decision circuit input for $|S_{mn}{\cdot}R_s|$=1000, $r = 0$ and $X_c = -14$ dB, for a) best BER and b) worst BER per MCF realization shown in Fig. 3 (a).

the received eye-patterns for $|S_{mn}{\cdot}R_s|$=0.01, $r = 0$ and $X_c = -16$ dB, for a) the best BER (1.85×10^{-5}) and b) the worst BER (1.175×10^{-1}) per MCF realization shown in Fig. 3 b). These eye patterns do not include

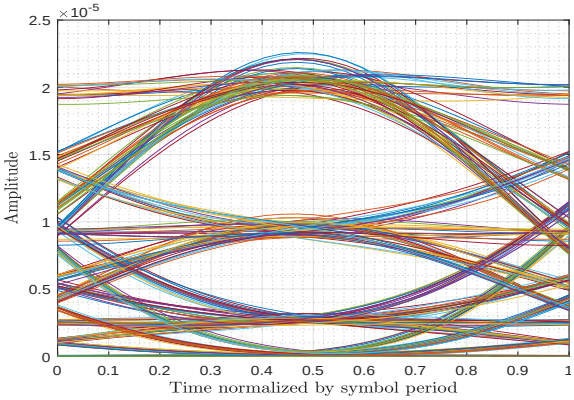

(a) BER=1.85×10^{-5}

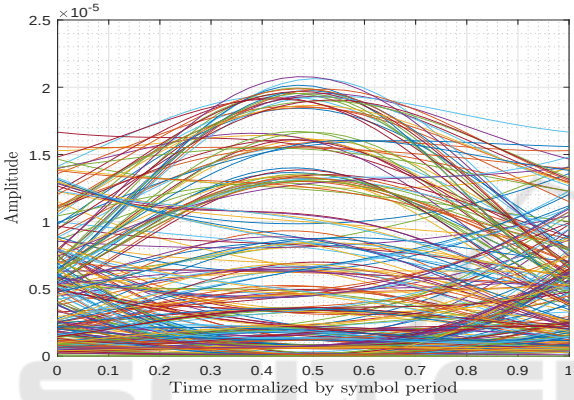

(b) BER=1.175×10^{-1}

Figure 5: Eye-Patterns at the decision circuit input for $|S_{mn}\cdot R_s|$=0.01, $r=0$ and $X_c=-16$ dB, for a) best BER and b) worst BER per MCF realization shown in Fig. 3 (b).

the effect of noise (electrical or optical) to make the effect of ICXT on the eye pattern more perceptible.

In Fig. 4 b) and 5 b), for the worst BER, due to the severe degradation caused by ICXT, the eye is fully closed. For the best BER, Fig. 5 a) exhibits much more "well-defined" amplitude levels caused by ICXT than in the eye-pattern shown in Fig. 4 a), especially in the part of the eye where more symbol transitions occur. There are two main reasons for this behavior: i) the ICXT level is 2 dB lower in Fig. 5 a), for low $|S_{mn}\cdot R_s|$. ii) for low $|S_{mn}\cdot R_s|$ (Fig. 5 a), only one symbol in the interfering core is contributing to ICXT, while for high $|S_{mn}\cdot R_s|$ (Fig. 4 a), several symbols in the interfering core are contributing to ICXT. A similar effect was observed for OOK systems (Rebola et al., 2019c) and PAM4 signals transmission impaired by ICXT induced by OOK signals in the interfered core (Jorge et al., 2020). Similar results and conclusions have been obtained for $r=0.1$. Furthermore, it has been found that, for $r=0.1$, the ICXT degrades less the average BER and received eye-patterns than for $r=0$.

3.3 Outage Probability

In this section, the dependence of the OP on the number of MCF realizations, MCF length, skew-symbol rate product and ICXT level is assessed.

3.3.1 Dependence on the Number of MCF Realizations

Fig. 6 shows the OP estimate as a function of the number of MCF realizations, for $r=0$, and and three different situations: a) $|S_{mn}\cdot R_s|$=1000 and $X_c=-18$ dB; b) $|S_{mn}\cdot R_s|$=0.01 and $X_c=-18$ dB and c) $|S_{mn}\cdot R_s|$=0.01 and $X_c=-22$ dB. To estimate the OP, the BER is obtained in each MCF realization and the simulation is stopped when the number of occurrences of BER above the BER limit reaches 200. According to Figs. 6 a) and b), it is possible to observe that for the same ICXT level and extinction ratio, a higher number of MCF realizations is required to reach 200 occurrences of BER above the BER limit, with $|S_{mn}\cdot R_s|$=1000 than with $|S_{mn}\cdot R_s|$=0.01, since the OP with $|S_{mn}\cdot R_s|$=1000 is about 1×10^{-2} and is lower than the OP of about 5×10^{-2} shown in Fig. 6 b), for $|S_{mn}\cdot R_s|$=0.01. In Figs. 6 a) and c), the number of MCF realizations to reach 200 BER occurrences above the BER limit is more than five times higher, in comparison to Fig. 6 b), and the oscillations of the OP estimates tend to diminish and stabilize above 10^4 MCF realizations, while in Fig. 6 b), the stabilization is reached after about 4000 realizations. Notice that in Fig. 6 c), the number of MCF realizations is considerably higher in comparison to Fig. 6 a) and b) cases, due to the lower OP (about one order of magnitude) that must be estimated. Fig. 6 indicates that the number of MCF realizations necessary to estimate the OP with sufficient accuracy only depends on the order of magnitude of the OP. A similar conclusion was shown in other works, for PAM4 and OOK signalling (Rebola et al., 2019c), (Jorge et al., 2020).

The number of occurrences for which it is possible to obtain an OP of the optical communication system with very small fluctuations has been assessed for this system, and it has been concluded that 200 occurrences of BER above the BER limit seem more than enough to achieve a stabilized estimate of outage probability. Thus, in all subsequent studies involving the OP estimation, N_o=200, are considered. The simulation results presented in this work only reach OPs around 10^{-4} because lower OPs are computationally heavy to achieve using computer simulation. To achieve an OP of 10^{-4} with 200 BER occurrences above the BER limit, around 2 million MCF realizations are required. As the estimation of the BER for one MCF realization takes around 0.6 seconds, around 2 weeks of simula-

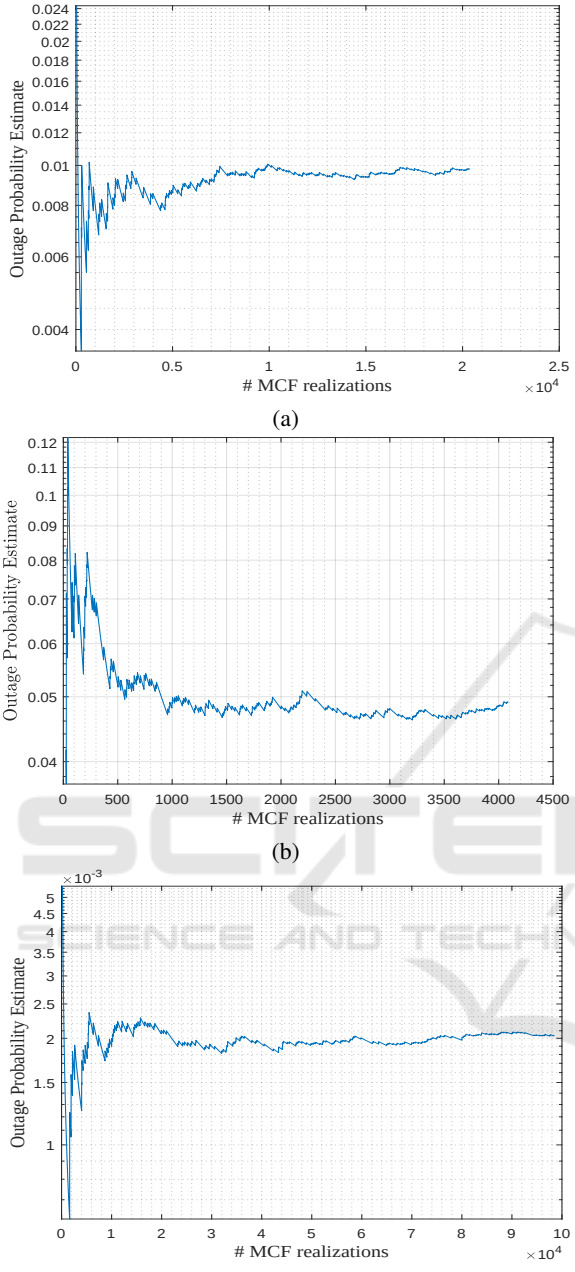

Figure 6: OP estimate as a function of the number of MCF realizations, for a MCF length of 10 km, $r = 0$ and a) $|S_{mn}{\cdot}R_s|$=1000 and $X_c = -18$ dB; b) $|S_{mn}{\cdot}R_s|$=0.01 and $X_c = -18$ dB and c) $|S_{mn}{\cdot}R_s|$=0.01 and $X_c = -22$ dB.

tion, in a 16 GB RAM with a 3.2 GHz processor are necessary to reach such low OPs. Therefore, for an OP of 10^{-6}, it would be necessary around 200 weeks. Similarly, we have performed a cubic interpolation and extrapolation of $\log_{10}$(OP), to achieve such low OPs, similarly to what has been done in (Rebola et al., 2019c), (Jorge et al., 2020).

3.3.2 Dependence on the Skew-Symbol Rate Product

The dependence of the OP on the skew-symbol rate product is studied with more detail in this subsection, for a MCF length of 80 km and $r = 0.1$.

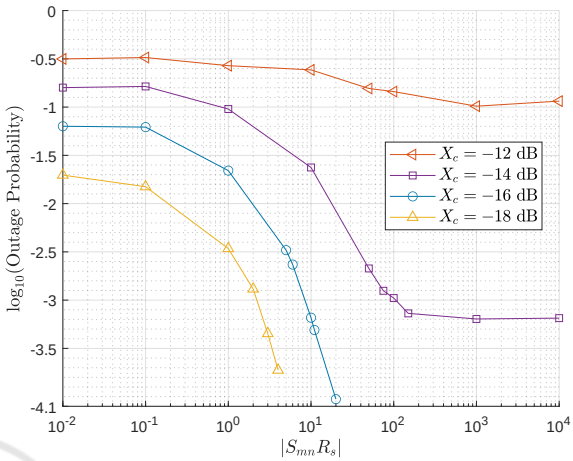

Figure 7: OP as a function of $|S_{mn}{\cdot}R_s|$ for a MCF length of 80 km, $r = 0.1$, and X_c=-12 dB, -14 dB, -16 dB and -18 dB.

For $|S_{mn}{\cdot}R_s| \ll 0.1$, the ICXT is highly correlated along the signal bandwidth (Alves and Cartaxo, 2019), only one PAM4 symbol is contributing to ICXT, and the ICXT behaves as static coupling (Alves and Cartaxo, 2019). Hence, the ICXT effect is enhanced and the OP reaches its worst-case value, concerning the skew-symbol rate product, for all ICXT levels studied. For $|S_{mn}{\cdot}R_s| \gg 100$, the ICXT is decorrelated along the signal bandwidth (Alves and Cartaxo, 2019) and several PAM4 symbols are contributing to ICXT, leading to a similar "noise"-like behavior (Alves and Cartaxo, 2019). Hence, a significant decrease of the OP is observed (Rebola et al., 2019c), (Rebola et al., 2019b), reaching a minimum for very high $|S_{mn}{\cdot}R_s|$. For intermediate values of the skew-symbol rate product, a transition between the two ICXT behaviors is observed, similarly to what has been reported in (Rebola et al., 2019b).

Fig. 7 also shows that, for X_c=-12 dB, the decrease of the OP is less than one order of magnitude when increasing the $|S_{mn}{\cdot}R_s|$. For X_c=-14, -16 and -18 dB, the OP decreases several orders of magnitude. These results show that, the OP improvement observed for high $|S_{mn}{\cdot}R_s|$ is smaller when the ICXT level increases, similarly to what has been concluded in (Rebola et al., 2019b), for an OOK system.

3.3.3 Dependence on the MCF Length

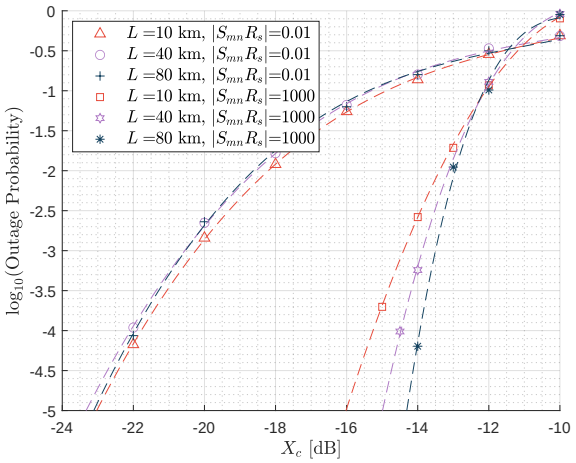

Figure 8: OP as a function of the ICXT level, for $|S_{mn}{\cdot}R_s|$=0.01 and $|S_{mn}{\cdot}R_s|$=1000, for $r = 0.1$. The dashed lines represent a cubic interpolation of $\log_{10}(\,)$ of the outage probability.

The dependence of the OP on the MCF length, and consequently, on the noise type dominance, i.e., electrical noise dominance or ASE noise dominance, for $|S_{mn}{\cdot}R_s|$=0.01 and $|S_{mn}{\cdot}R_s|$=1000, $r = 0.1$, and several ICXT levels, is studied in this subsection. In this study, we aim to analyse the effect of the ICXT on these environments. Therefore, the ICXT level is set constant for each fiber length, i. e., the ICXT level is considered independent of the MCF length. Fig. 8 shows the OP as a function of the ICXT level, for $|S_{mn}{\cdot}R_s|$=0.01 and $|S_{mn}{\cdot}R_s|$=1000, for $r = 0.1$ and L=10 km, L=40 km and L=80 km. In Fig. 8, for high $|S_{mn}{\cdot}R_s|$, longer MCF lengths lead to an increased tolerance to ICXT, while for low $|S_{mn}{\cdot}R_s|$, the ICXT tolerance is not significantly affected by the MCF length. Hence, for high $|S_{mn}{\cdot}R_s|$, the difference between the dominance of signal-ASE beat noise on the performance, for 80 km, and the enhanced contribution of electrical noise to the performance, for 10 km, influences the tolerance to ICXT. For low $|S_{mn}{\cdot}R_s|$, the tolerated ICXT level is not particularly affected by the different noise regimes.

The ICXT levels that lead to an OP of 10^{-4}, for each intercore skew and MCF length combination, extracted from Fig. 8, are presented in Table 2. In Table 2, for $|S_{mn}{\cdot}R_s|$=0.01, the ICXT level required to achieve an OP of 10^{-4} increases slightly less than 0.5 dB, with the MCF length increase. For $|S_{mn}{\cdot}R_s|$=1000, the maximum acceptable ICXT level required to achieve the OP of 10^{-4} diminishes with the MCF length increase, showing a 0.8 dB and 1.4 dB reduction from 40 km and 80 km, respectively, to 10 km. For 80 km, for an OP of 10^{-4}, a higher tolerance to ICXT exceeding 8.1 dB is observed for high $|S_{mn}{\cdot}R_s|$ in comparison to low $|S_{mn}{\cdot}R_s|$. The way dispersion from the MCF and DCF affects the ICXT mechanism for the different link lengths might provide some explanation for these results. Even though, for an OP of 10^{-4}, the maximum acceptable ICXT level shows only a variation not exceeding 1.4 dB with the increase of the MCF length.

Table 2: Maximum acceptable ICXT level (dB) for an OP of 10^{-4} and $r = 0.1$.

	L=10 km	L=40 km	L=80 km
$\|S_{mn}R_s\|$=0.01	-21.8	-22.1	-22
$\|S_{mn}R_s\|$=1000	-15.3	-14.5	-13.9

4 CONCLUSIONS

In this work, the impact of ICXT induced by one interfering core on the performance of an optically amplified PAM4 IM-DD system with full loss and chromatic dispersion compensation was studied through MC simulation by assessing the average BER, eye-pattern degradation, and OP.

We have shown that 1000 MCF realizations are more than enough to obtain stabilized average BERs and that is essential to study the OP for IM-DD systems supported by MCFs impaired by ICXT. For low $|S_{mn}{\cdot}R_s|$, the eye-patterns exhibit more "well-defined" amplitude levels due to ICXT in comparison to high $|S_{mn}{\cdot}R_s|$. Furthermore, for $r = 0.1$, the ICXT degrades less the average BER and received eye-patterns than for $r = 0$. For an OP of 10^{-4}, numerical results have shown a higher tolerance to ICXT exceeding 8.1 dB is observed for high $|S_{mn}{\cdot}R_s|$. It has also been shown that, with the ICXT level independent from the MCF length, the OP is not much affected by increasing the MCF length, from 10 km, where electrical noise significantly contributes to the performance degradation, to 80 km, where signal-ASE beat noise is dominant. From a MCF length of 10 to 80 km, and to achieve the typical OP of 10^{-4}, the maximum acceptable ICXT level varies only 1.4 and 0.2 dB, respectively, for $|S_{mn}{\cdot}R_s|$=1000 and $|S_{mn}{\cdot}R_s|$=0.01.

This work demonstrates that in optically amplified PAM4 IM-DD system supported by MCFs, the ICXT level must be kept below -22 dB to guarantee an OP$\leq$ 10^{-4}. If the ICXT level exceeds this threshold, ICXT mitigation techniques should be developed to maintain the quality of transmission.

ACKNOWLEDGEMENTS

This work is funded by FCT/MCTES through national funds and when applicable co-funded EU funds under the project UIDB/EEA/50008/2020 and project DigCore/UIDP/50008/2020.

REFERENCES

Agrawal, G. (2010). *Fiber-optic communications systems*. John Wiley & Sons, 4^{th} edition.

Alves, T. M. F. and Cartaxo, A. V. T. (2017). Intercore crosstalk in homogeneous multicore fibers: theoretical characterization of stochastic time evolution. *Journal of Lightwave Technology*, 35, no. 21:4613–4623.

Alves, T. M. F. and Cartaxo, A. V. T. (2019). Decorrelation bandwidth of intercore crosstalk in weakly coupled multicore fibers with multiple interfering cores. *Journal of Lightwave Technology*, 37, no. 3:744–754.

Alves, T. M. F., Rebola, J., and Cartaxo, A. V. T. (Mar. 2019). Outage probability due to intercore crosstalk in weakly-coupled MCF systems with OOK signaling. *Optical Fiber Communications Conference and Exhibition (OFC)*, San Diego, CA, USA, paper M2I.1.

Butler, D., Li, M.-J., Li, S., Geng, Y., Khrapko, R., et al. (2017). Space division multiplexing in short reach optical interconnects. *Journal of Lightwave Technology*, 35, no. 4:677–682.

Carlson, A. and Crilly, P. (2010). *Communication Systems - An introduction to signals and noise in electrical communication*. McGraw-Hill International Editions, New York, USA, 5^{th} edition.

Cartaxo, A. V. T., Luís, R. S., Puttnam, B. J., Hayashi, T., Awaji, Y., et al. (2016). Dispersion impact on the crosstalk amplitude response of homogeneous multicore fibers. *IEEE Photonics Technology Letters*, 28, no. 17:1858–1861.

Cisco (2018). Cisco global cloud index: forecast and methodology, 2016–2021. *White paper*, pages 1–46.

Cvijetic, N., Wilson, S., and Qian, D. (2008). System outage probability due to PMD in high-speed optical OFDM transmission. *Journal of Lightwave Technology*, 26, no. 14:2118–2127.

El-Fiky, E., Chagnon, M., Sowailem, M., Samani, A., Morsy-Osman, M., et al. (2017). 168 Gb/s single carrier PAM4 transmission for intra-data center optical interconnects. *IEEE Photonics Technology Letters*, 29, no. 3:314–317.

Jorge, I., Rebola, J. L., and Cartaxo, A. V. T. (2020). Transmission of PAM4 signals in ICXT-impaired intra-datacenter connections with PAM2 signal interference. In *International Conference of Photonics, Optics and Laser Technology (Photooptics)*, pages 122–130, Valletta, Malta.

Kachris, C. and Tomkos, I. (2012). A survey on optical interconnects for data centers. *IEEE Communications Surveys Tutorials*, 14, no. 4:1021–1036.

Klaus, W., Puttnam, B. J., Luis, R. S., Sakaguchi, J., Mendinueta, J. D., et al. (2017). Advanced space division multiplexing technologies for optical networks. *IEEE/OSA Journal of Optical Communications and Networking*, 9, no. 4:1–11.

Luís, R. S., Puttnam, B. J., Cartaxo, A. V. T., Klaus, W., Mendinueta, J. M. D., et al. (2016). Time and modulation frequency dependence of crosstalk in homogeneous multi-core fibers. *Journal of Lightwave Technology*, 34, no. 2:441–447.

Noormohammadpour, M. and Raghavendra, C. S. (2018). Datacenter traffic control: understanding techniques and tradeoffs. *IEEE Communications Surveys Tutorials*, 20, no. 2:1492–1525.

Perin, J., Anujit, S., and Kahn, J. (2018). Data center links beyond 100 Gbit/s per wavelength. *Optical Fiber Technology*, 44, no. 1:69–85.

Rademacher, G., Luís, R. S., Puttnam, B. J., Awaji, Y., and Wada, N. (2017). Crosstalk dynamics in multi-core fibers. *Optics Express*, 25, no. 10:12020–12028.

Rebola, J. L., Alves, T. M. F., and Cartaxo, A. V. T. (2019a). Assessment of the combined effect of laser phase noise and intercore crosstalk on the outage probability of DD OOK systems. In *International Conference on Transparent Optical Networks (ICTON)*, Angers, France, paper We.D1.4.

Rebola, J. L. and Cartaxo, A. V. T. (2000). Optimization of level spacing in quaternary optical communication systems. In *International Conf. on Applications of Photonic Technology*, volume 4087, pages 49–59, Otava, Canadá.

Rebola, J. L., Cartaxo, A. V. T., Alves, T. M. F., and Marques, A. (2019b). Outage probability due to intercore crosstalk in dual-core fiber links with direct-detection. *IEEE Photonics Technology Letters*, 31, no. 14:1195–1198.

Rebola, J. L., Cartaxo, A. V. T., and Marques, A. (2019c). 10 Gbps CPRI signals transmission impaired by intercore crosstalk in 5G network fronthauls with multicore fibers. *Photonic Network Communications*, 37, no. 3:409–420.

Soeiro, R. O. J., Alves, T. M. F., and Cartaxo, A. V. T. (2017). Dual polarization discrete changes model of inter-core crosstalk in multi-core fibers. *IEEE Photonics Technology Letters*, 29, no. 16:1395–1398.

Winzer, P. and Foschini, G. (2011). MIMO capacities and outage probabilities in spatially multiplexed optical transport systems. *Optics Express*, 19, no. 17:16680–16696.

Xing, Z., Samani, A., Xiang, M., El-Fiky, E., Hoang, T. M., et al. (2018). 100 Gb/s PAM4 transmission system for datacenter interconnects using a SiP ME-MZM based DAC-less transmitter and a VSB self-coherent receiver. *Optics Express*, 26, no. 18:23969–23979.

Zhou, X., Urata, R., and Liu, H. (2019). Beyond 1 Tb/s datacenter interconnect technology: challenges and solutions. *Optical Fiber Communications Conference and Exhibition (OFC)*, San Diego, CA, USA, paper Tu2F.5.